Tuning Nitrogen Content in ZIF 67 Derived Porous Carbon for Efficient Room-Temperature Hydrogen Storage

Dhanya A R[1], Sana Fathima T K[1], Sundara Ramaprabhu[1]*

[1]Alternative Energy Nanotechnology Laboratory (AENL), Department of Physics, Indian Institute of Technology Madras, Chennai 600036, Tamil Nadu, India

** Corresponding author Email: ramp@iitm.ac.in*

Abstract

Hydrogen is considered a promising alternative to fossil fuels, but its storage challenges impede its widespread adoption. Researchers are exploring various porous materials, including metal-organic frameworks (MOFs), to develop effective hydrogen storage solutions at room temperature and reasonable pressures. Materials derived from MOFs can be tuned for desirable properties like high surface area, permanent porosity, and high thermal and chemical stability, making them excellent hosts for hydrogen molecules. Here, a mixture of ZIF 67 and different compositions of melamine is carbonized at a high temperature (800°C) to obtain ZIF 67 derived Co/NC, Co/NC-0.3, Co/NC-0.5 and Co/NC-1. Phase, morphology, and composition are confirmed through various characterizations. The hydrogen storage studies are conducted within the temperature range of 25-100°C and at pressures 5-18 bar. Co/NC-0.5 is observed to have the hydrogen storage capacity among all the samples at 16 bar, 25°C. The factors that contribute to the enhancement of hydrogen storage capacity in Co/NC-0.5 are the large surface area, defects produced on ZIF-derived structures due to uniform N doping, and the presence of Co nanoparticles (NPs) embedded in the porous support. The main mechanism involved here is the spillover and physisorption for the dissociation of the hydrogen molecules into atoms on Co NPs and its diffusion in the carbon matrix.

Keywords: *hydrogen storage, Co/NC, ZIF 67-derived, porous carbon, spillover mechanism*

1. Introduction

For a considerable amount of time, hydrogen has been considered the best alternative energy carrier that could eventually replace the use of fossil fuels. The absence of a reliable and secure storage mechanism prevents hydrogen from being used as fuel on a large scale [1]. Ongoing research has put efforts into studying hydrogen storage in different porous materials at cryogenic temperatures, whereas the major challenge is to store it at room temperature and under reasonable pressure conditions. Metal-organic frameworks (MOFs) and derived MOFs are some promising candidates that can be utilized to store hydrogen under these conditions [2-6].

By carefully selecting metal clusters and organic ligands, metal-organic frameworks (MOFs) with high specific surface area (SSA), high porosity, high thermal and chemical stability, abundant active sites, and long-range organized crystalline structure can be formed. Because of these characteristics, MOF is a promising host for several functional guest molecules, such as metal oxide or noble metal nanoparticles [3,7-8]. The MOF composites have been studied in applications that include hydrogen adsorption, carbon dioxide (CO_2) sequestration, heterogeneous catalysis, carbon dioxide conversion, etc, wherein properties such as high Specific Surface Area (SSA), dispersion in nanoparticles (NPs) and potential active surface functionalities properties are utilized. It is also reported that MOFs can be used as standard supports for noble metal NP doping in microporous/channel-like structures or MOF metal clusters, improving their heterogeneous catalytic ability [2,9].

Maintaining MOF purity for metal doping in an aqueous environment is difficult because metal NPs may form agglomerations on MOF exterior

surfaces. An alternative to noble metal is also required [10,11]. Thus, the idea of pyrolyzing MOFs to produce MOF-derived carbons (MDCs) started to take shape. These MOF-derived carbons are reported to contain metal/metal oxide nanoparticles formed from metal clusters, focusing on their preparation, structure, and applications. The advantage of MOF-derived catalysts is that they preserve the MOF precursor's high porosity, large specific surface area, and highly organized structure [12]. Zeolitic imidazolate framework (ZIF) materials, in particular, are thought to be the most promising precursors for the creation of M-N-C catalysts because they contain enough well-ordered nitrogen and metal atoms in the framework that can be utilized in hydrogen adsorption. Lu et al. observed good hydrogenation catalytic activity due to hydrogen spillover on Pd-Co active sites and nitrogen doping from 2-methylimidazole (2-mIm) ligand in the Pd-Co/ZIF-derived carbon (ZDC) [13]. Co/ZDCs are reportedly used as catalysts for hydrogenation reactions without adding noble metals [14,15].

One of the major mechanisms in hydrogen storage is the spillover mechanism, wherein hydrogen molecules get dissociated into their respective atoms, which then get weakly chemisorbed on the metal nanoparticles decorated carbon support. These dissociated atoms then diffuse towards the support via a secondary spillover effect, enabling effective hydrogenation of the catalyst. This mechanism has been reported for many MOF-based materials; for example, in Pt/NH_2MIL-125(Ti), it has been reported for photocatalytic CO_2 reduction to formate [16]. Both noble and non-noble metal nanoparticles are reportedly used as hydrogen spillover sources. So, from these metal nanoparticle catalysts where the dissociation of H_2 molecules occurs, diffuses within the porous carbon support, and these H atoms occupying the porous carbon sites with a large change in enthalpy of formation is the most desirable for the room temperature hydrogen storage. Li et al. [17] reported hydrogen storage capacity as 1 wt% for Pt on MOFs, the first MOF to be reported for hydrogen storage. Tsao et al. [18] observed that the size of the Pt cluster affects the H diffusion distance within the support, and as the size decreases, it results in a longer spillover, which leads to a larger H diffusion distance.

To deposit N-doped microporous ZDC without noble metals, we pyrolyzed ZIF 67 at higher temperatures for carbonization at a particular ramp rate. Co-aggregation can be prevented by low pyrolytic temperatures, but due to insufficient thermal energy, it will not carbonize ZIF 67. In addition to Co aggregation, porosity is drastically lost at very high ZIF pyrolysis temperatures in inert gas. The fast-ramping process circumvents ZIF decomposition and excessive catalyst size, preventing the spillover mechanism necessary to enhance hydrogen storage [4].

In this work, ZIF 67 is chosen as the material for the hydrogen storage studies. Zeolitic Imidazolate Frameworks (ZIF) is a subclass of Metal-Organic frameworks built by tetrahedral metal cations M (M = Zn or Co) and imidazolate ligands (Im). ZIF-67 (Co $(Hmim)_2$, Hmim = 2-methylimidazole) consists of cobalt ion (Co^{2+}) and 2-methylimidazolate anions and exhibits a cubic crystal symmetry with unit cell parameters of $a = b = c = 16.9589$ Å with a morphology of rhombic dodecahedron. ZIF 67 was synthesized using a slightly modified technique, reported by Fathima et al. [19]. Then, ZIF 67 and the appropriate addition of melamine were carbonized at high temperatures to synthesize Co/NC, Co/NC-0.3, Co/NC-0.5, and Co/NC-1. These samples were then characterized to investigate the phase, morphology, structure, and composition. Hydrogen storage studies were conducted, and the performance was compared for all the samples.

2. Experimental

2.1. Synthesis

A modified synthesis technique, reported by Sana et al. in previous work, was used to prepare ZIF 67. The combination of methanol and 2-methylimidazole solution (45 mmol) was added to another mixture of methanol and cobalt nitrate hexahydrate solution (5.74 mmol) under constant stirring at room temperature. An overnight stirring of the solution

was kept at room temperature. It was then filtered, washed twice with methanol, and dried at 60 °C to get a purple powder labeled as ZIF67 [19]. The schematic is shown in Fig 1.

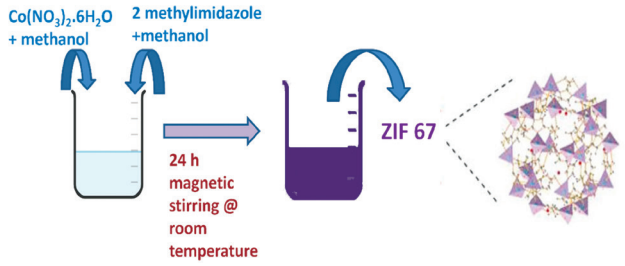


Fig. 1. Schematic of the synthesis of ZIF 67

Co/NC samples were synthesized using the pyrolysis technique. Initially, the as-synthesized ZIF 67 (mentioned in the previous paragraph) was mixed with x amount of melamine (x denotes x mmol of melamine added to 0.8 g of ZIF 67). These samples were labeled ZIF 67+0.3 mmol MEL, ZIF 67+0.5 mmol MEL, and ZIF 67+1 mmol MEL, respectively. These samples were then pyrolyzed at 800°C for 2 hrs in the nitrogen atmosphere. Then, the final samples were denoted as Co/NC-0.3, Co/NC-0.5, and Co/NC-1, respectively, where 0.3, 0.5, and 1 denote the amounts of melamine (in mmol) added to ZIF 67 before carbonization. Pure Co/NC was synthesized without adding melamine and pyrolyzing ZIF 67 at 800°C for 2 hrs in the N_2 atmosphere. A sodalite-type MOF-based structure where Co^{2+} and 2-MIM are regularly arranged is obtained in the powder form [6]. The schematic of the synthesis of derived carbon from ZIF 67 is as shown in Fig 2.

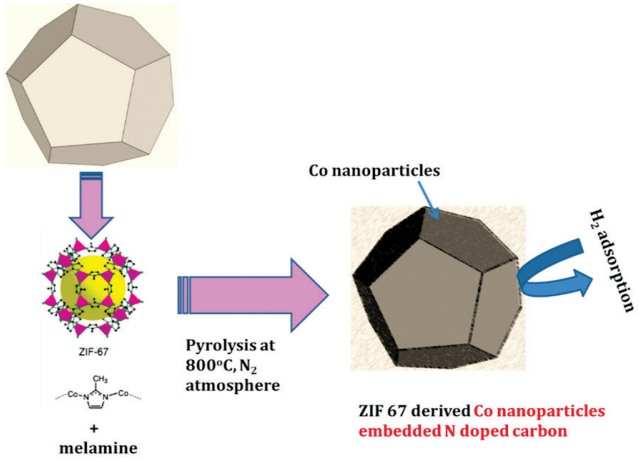


Fig. 2. Schematic of the synthesis of Co/NC, Co/NC-0.3, Co/NC-0.5, and Co/NC-1

2.2. Characterization Techniques

For X-ray diffraction (XRD) studies, a Rigaku Smartlab Diffractometer with Cu Kα radiation and nickel filter (λ=0.154nm, 40 kV, and 100mA) was used. Using TA equipment, the SDT-Q600, thermogravimetric analysis (TGA) was performed at 20°C per minute in an air atmosphere. FTIR spectra were obtained using the Agilent Technologies Cary 630 FTIR. Horiba XPLORA-MV2000 Raman spectrometer with 488 nm laser wavelength was employed to obtain the Raman spectra. Energy Dispersive X-ray Spectra (EDAX) and Field Emission Scanning Electron Microscopy (FESEM) images were measured using the Inspect F Scanning Electron Microscope (SEM). Using the Micromeritics ASAP 2020 surface area and porosity analyzer, the specific surface area (SSA), pore volume, and pore size distribution data of all the ZIF 67 derived samples were extracted. The nitrogen adsorption/desorption isotherms at 77K were used to analyze the data using the Brunauer-Emmett-Teller (BET) and Barrett-Joyner-Halanda (BJH) theories.

2.3. Hydrogen Storage Measurements

A high-pressure Sieverts apparatus was used to test the hydrogen storage capacity of the Co/NC-based samples using the volumetric technique of analysis. The number of moles of hydrogen adsorbed by the sample was determined using van der Waal equations for the real gas. Before volume calibration and degassing, a leak check procedure was performed on the system. Degassing is done at a high vacuum (10^{-6} mbar) for two hours at a temperature of roughly 200 °C following the volume calibration. After the system's temperature is adjusted to a desired level, hydrogen is then let to enter the system. For the purpose of calculating the number of moles of hydrogen interacting with the sample, the initial and equilibrium pressures are recorded. To prevent any errors in the pressure readings that can be caused by changes in the ambient temperature conditions, room temperature is maintained at 24±1°C values throughout the experiment.

3. Results and Discussions

The XRD pattern of as-synthesized ZIF 67 particles, as shown in Fig 3 (a), matches well with the reported XRD pattern of ZIF 67.[20] In Fig 1(b), the patterns of Co/NC, Co/NC-0.3, Co/NC-0.5, and Co/NC-1 samples, which are derived from different compositions of melamine along with ZIF 67, match the pattern of Co that has an fcc phase. The XRD peaks of all the samples in Fig 1(b) at 44.3°, 51.6°, and 75.9° correspond to (111), (200), and (220) of the Co nanoparticles embedded within the ZIF 67-derived nitrogen-doped porous carbon [14]. The very low intensity of the Co peaks and no obvious peaks of graphitized carbon are observed, which indicates low crystallization of Co_3O_4 and amorphous carbon. The formation of Co_3O_4 is reported at high pyrolysis temperature of ZIF 67-based material (800˚C and above) due to the crystallization of amorphous Co_3O_4. Here, since we do not observe the peaks of Co_3O_4 in all the samples pyrolyzed at 800˚C, this indicates a low crystallization of amorphous Co_3O_4 that leads to the formation of Co nanoparticles within the carbon matrix.

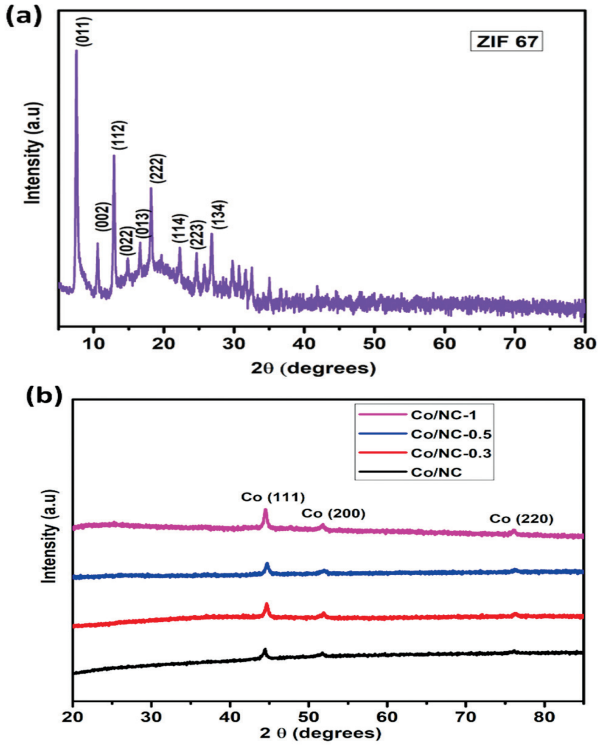


Fig. 3. XRD of (a) ZIF 67 before pyrolysis (b) ZIF 67 and melamine derived Co/NC, Co/NC-0.3, Co/NC-0.5, and Co/NC-1

In the Raman spectra, as shown in Fig 4, Co/NC, Co/NC-0.3, Co/NC-0.5, and Co/NC-1 exhibited two well-defined peaks approximately at 1327-1350 cm^{-1} and 1580-1600 cm^{-1} that belongs to the D and G bands of the graphitic carbon. This confirms the presence of carbon in all the ZIF 67-derived Co/NC samples. The ratio of I_D to I_G shows the degree of structural disorder in carbon-based nanocomposites. The higher the I_D/I_G value, the lower the graphitization of the sample and the higher the presence of the defects [21]. As seen from Fig 4, the I_D/I_G value is higher for Co/NC-0.5 when compared with other samples; thus, it has more structural defects. Adding melamine to the ZIF 67 creates more defects at higher annealing temperatures (800˚C). The defects come from the N atoms within the sample, which are contributed by the decomposition of melamine. Although a higher amount of melamine is used to prepare the Co/NC-1 sample, Co/NC-0.5 shows the optimum number of defects necessary to disperse a higher number of Co nanoparticles within the carbon matrix without the loss of dodecahedron structure of ZIF 67-based material. For Co/NC-1, we observe the distortion of the sodalite cage structure of ZIF 67 particles (as seen from the SEM images), although more N atoms are present, which can lead to the agglomeration of these Co nanoparticles and reduced surface area of the carbon support.

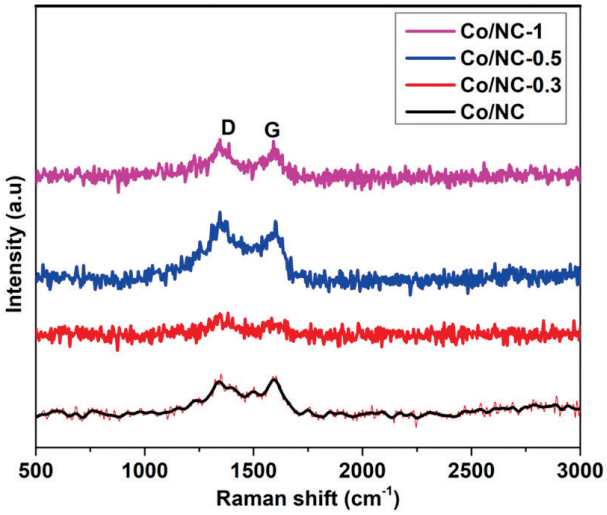
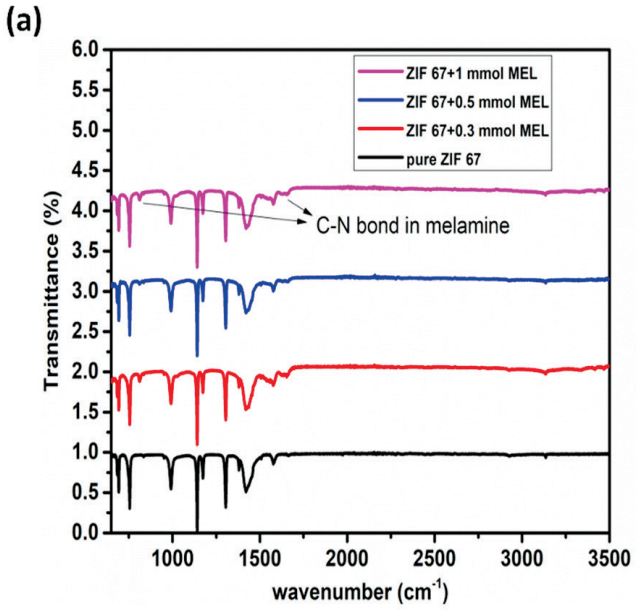


Fig. 4. Raman spectra of Co/NC, Co/NC-0.3, Co/NC-0.5 and Co/NC-1

ZIF 67 before pyrolysis, along with different compositions of melamine, has many IR peaks within the range 600-1700 cm^{-1}, as shown in Fig 5 (a). These peaks indicate the presence of ZIF 67, and the presence of melamine is also indicated by the C-N bond peaks, as seen in Fig 5(a). The absorption peaks at 1500-600 cm^{-1} are the characteristic peaks of the imidazole ring and the peak at 1578 cm^{-1} is ascribed to the stretching mode of C-N in imidazole. The IR peaks at 3100 cm^{-1} and 2900 cm^{-1} indicate the C-H stretching vibrations in the methyl group and imidazole ring [22]. The peaks that indicate the stretching vibration and out-of-plane bending modes of the C-N bond are present only in the ZIF 67 samples containing melamine at ~1600 cm^{-1} and 800 cm^{-1} [23]. When ZIF 67 is pyrolyzed at 800 °C, all the characteristic peaks of ZIF 67 disappear in all the samples. The ZIF 67 derived Co/NC, Co/NC-0.3, Co/NC-0.5, and Co/NC-1 exhibit IR peaks at 1600 cm^{-1}, which is attributed to the vibration of the graphitic carbon, as seen in Fig 5(b). The peaks observed at 1900 cm^{-1}, 2000 cm^{-1} and 2200 cm^{-1} belong to -C≡C-, as seen in Fig 5(b) are originating from the diamond crystal used in the FTIR instrument [24].



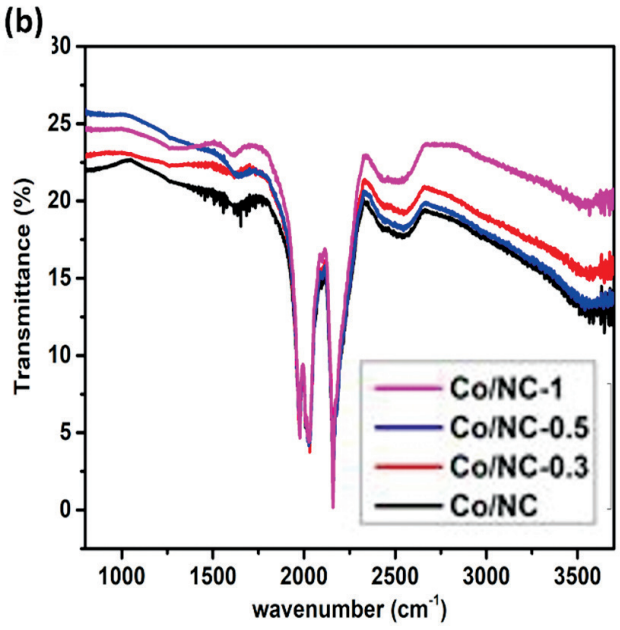


Fig. 5. FTIR of (a) ZIF 67, ZIF67+0.3 mmol MEL, ZIF67+0.5 mmol MEL and ZIF67+1 mmol MEL (b) Co/NC, Co/NC-0.3, Co/NC-0.5 and Co/NC-1

Thermogravimetric analysis was performed for ZIF 67, ZIF 67+0.3 mmol MEL, ZIF 67+0.5 mmol MEL, and ZIF67+1 mmol MEL in a nitrogen atmosphere from room temperature to 1000°C at a rate of 20°C/min, as shown in Fig 6. The graph shows two peaks that indicate weight loss, one between 200°C and 400°C and the other between 400°C and 600°C. The adsorption of the water molecules on the surface causes weight loss, which is observed at 250-300°C for melamine-added ZIF 67 samples. The decomposition of melamine starts at 300°C and is decomposed completely above 400°C [6]. The decomposition temperature of the samples reduces with the presence of melamine, indicating that adding melamine to ZIF 67 could accelerate the decomposition of ZIF 67 [4,6]. The weight loss of ZIF 67+0.5 mmol MEL and ZIF 67 is lower than that of ZIF 67+0.3 mmol MEL and ZIF 67+1 mmol MEL, indicating that the interaction between melamine and ZIF 67 is more in ZIF 67+0.5 mmol MEL. The weight percent of Co is observed to be the highest for ZIF 67+0.5 mmol MEL (~27 wt%).

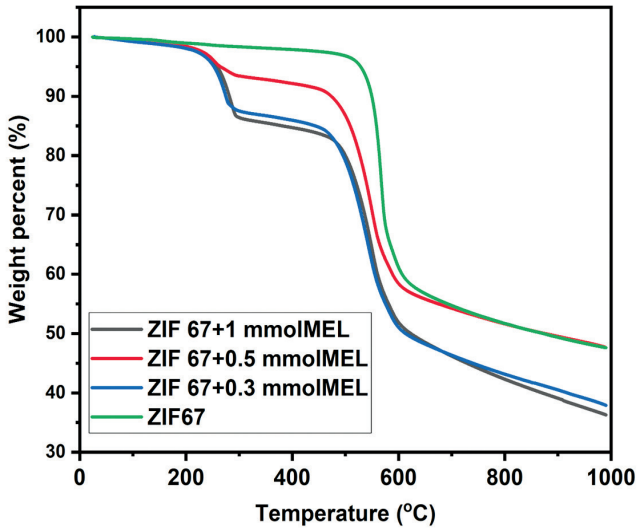


Fig. 6. TGA of ZIF 67, ZIF 67+0.3 mmol MEL, ZIF 67+0.5 mmol MEL, and ZIF 67+1 mmol MEL

It is observed from Fig 7 that after pyrolysis of ZIF 67 to 800°C, in SEM images, the ZIF particles with sodalite cage pore structure or rhombic-dodecahedron structure are distorted, and the surfaces are rough**.** For the samples Co/NC-0.3 and Co/NC-0.5, the growth of small carbon nanotubes is observed at the distorted edges of the particles. When melamine is 1mmol, more round particles can be seen embedded in the matrix where the surface has become rougher, and there is a complete distortion of the sodalite cage structure of ZIF 67 particles at the same annealing temperature in the Co/NC-1 sample [25]. Table [S1-S4] shows the EDAX spectra and elemental composition of Co/NC, Co/NC-0.3, Co/NC-0.5, and Co/NC-1. The lowest nitrogen content and the highest Co content are observed for the Co/NC-0.5 sample, as seen in Table S4. This confirms that the interaction between melamine and ZIF 67 is greater in ZIF 67+0.5 mmol MEL, as indicated by the TGA results since the content of Co is highest in this sample. Co/NC-0.5 also shows less distortion of the edges of the structure (Fig 7(c)) and thus maximizes the uniform distribution of Co nanoparticles within it.

The presence of amorphous carbon is seen in SEM images (Fig 7 [a-d]) for all the Co/NC samples but the amount is less due to less amount of melamine taken in comparison with the ZIF 67. For all the ZIF 67 derived samples, we observe a quite large surface area, as seen from BET isotherm graphs (Fig 8 (a)). The largest surface area is observed for Co/NC-0.5, which indicates that it can accommodate more hydrogen atoms that get diffused within the carbon after the dissociation of hydrogen molecules due to its interaction with the Co nanoparticles via the spillover effect.

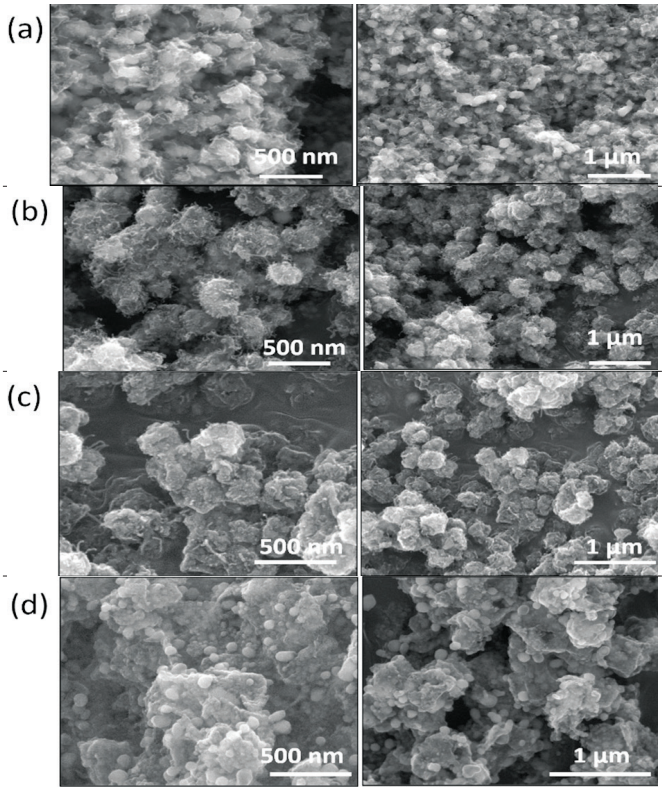


Fig .7. SEM of (a) ZIF 67 (b) Co/NC-0.3 (c) Co/NC-0.5 (d) Co/NC-1

The BET isotherms and pore size distribution plots for the samples Co/NC, Co/NC-0.3, Co/NC-0.5, and Co/NC-1 are shown in Fig 8 (a) and (b). Type IV isotherm is observed for all the samples, as seen in Fig 8 (a), which is characteristic of mesopores. The highest specific surface area (372.6900 m^2/g) and pore volume (0.4290 cm^3/g) are observed for Co/NC-0.5. In the pore size distribution plots, as shown in Fig 8 (b), the pore diameter peak is observed at less than 5 nm for Co/NC, Co/NC-0.3, and Co/NC-0.5, but above 2 nm, which indicates the presence of mesopores within the carbon matrix in these samples [26]. For Co/NC-1, it is observed that the pore diameter is the highest among all, indicating

the presence of macropores and mesopores. Co/NC has the highest SSA and pore volume and the lowest pore width/diameter, so the presence of active sites for the physisorption of hydrogen molecules will be the highest among all samples. Table 1 shows all the BET parameters that show SSA, pore volume, and pore diameter of all samples.

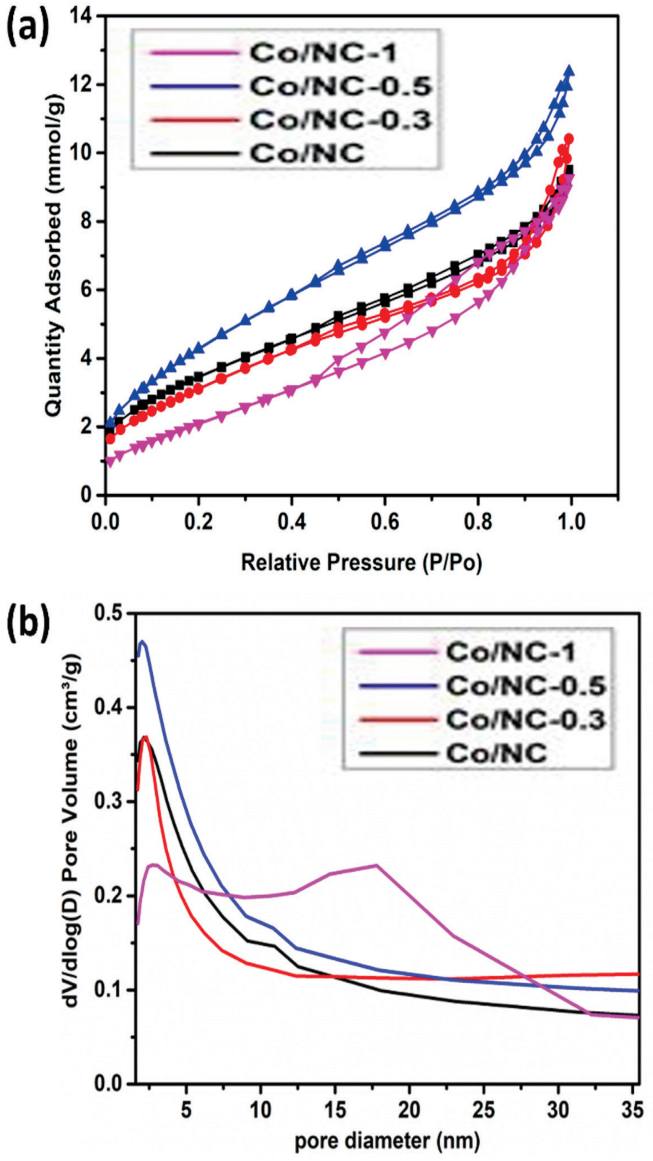


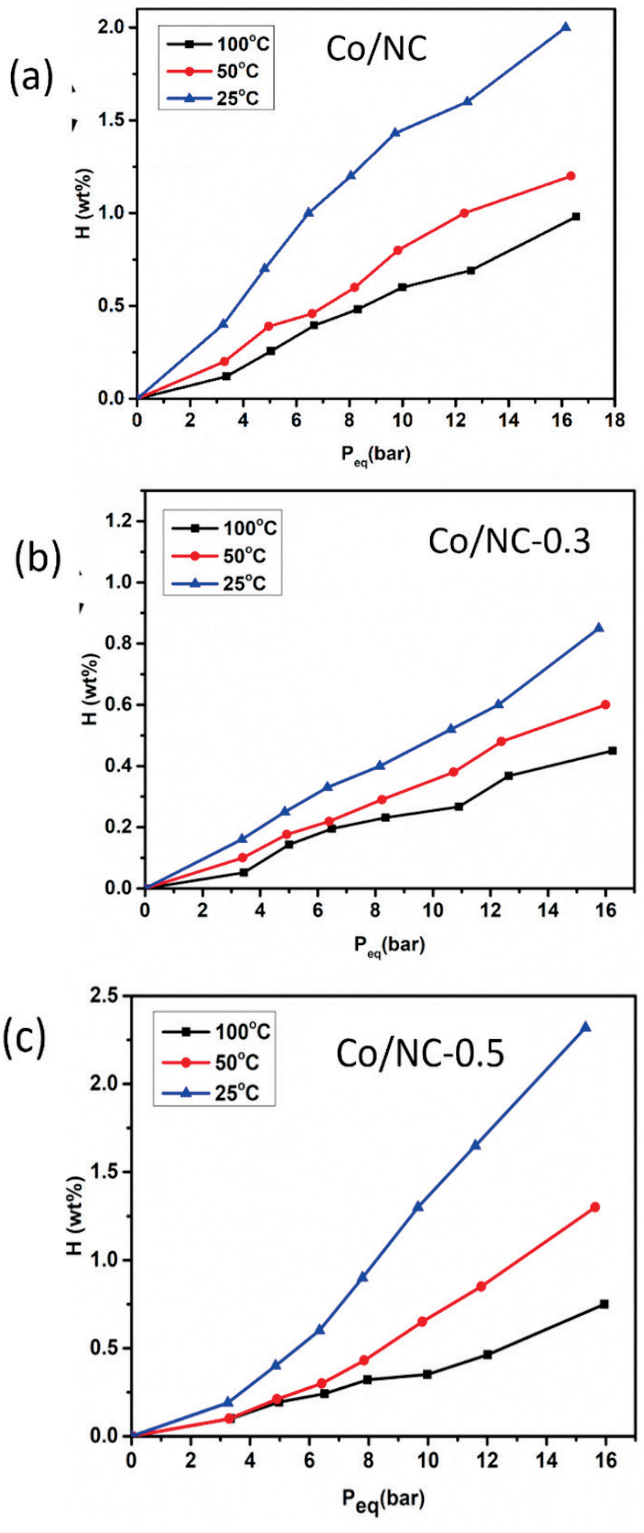
Fig. 8 (a) BET isotherms and (b) pore size distribution plot of Co/NC, Co/NC-0.3, Co/NC-0.5, and Co/NC-1

Table 1 BET parameters SSA, pore volume, and pore diameter of Co/NC, Co/NC-0.3, Co/NC-0.5, and Co/NC-1

S N	Sample	SSA (m^2/g)	Pore volume (cm^3/g)	Pore diameter (nm)
1.	Co/NC	289.0686	0.329866	4.56453
2.	Co/NC-0.3	268.9454	0.360945	5.36830
3.	Co/NC-0.5	372.6900	0.429009	4.60446
4.	Co/NC-1	191.3495	0.320949	6.70918

The hydrogen adsorption properties of Co/NC, Co/NC-0.3, Co/NC-0.5, and Co/NC-1 were performed using a high-pressure Sievert's apparatus.[27]. The temperature and pressure ranges for the measurements were from 25–100°C and 5–18 bar, respectively. The pressure-composition (PC) isotherm plots for all the samples are shown in Fig 9 [a-d]. From these plots, it is depicted that the hydrogen storage capacities of Co/NC, Co/NC-0.3, Co/NC-0.5, and Co/NC-1 are 2 wt%, 0.8 wt%, 2.4wt%, and 1.3 wt% at 16 bar and 25°C, respectively. The hydrogen adsorption capacity linearly increases with the pressure at a particular temperature. This is indicative of the physisorption occurring within the carbon matrix. The maximum physisorption occurs for the material having a large surface area, which is the highest for Co/NC-0.5, according to the BET results. The interaction between melamine and ZIF 67 is more in Co/NC-0.5, according to TGA of ZIF 67+0.5 mmol MEL and EDAX of Co/NC-0.5, which results in the maximum coordination between N and C. This makes the distribution of Co nanoparticles in Co/NC-0.5 more uniform throughout the material. This enhances the hydrogen spill-over effect over these Co nanoparticles embedded within the nitrogen-doped carbon matrix. According to TGA, the weight percent of Co is high in Co/NC-0.5, which indicates that the hydrogen molecules interact with more Co nanoparticles in this case. This leads to the improvement in the storage capacity of ZIF 67-derived Co/NC-0.5. The carbon matrix alone would exhibit limited hydrogen storage capacity due to weak van der Waal's forces between hydrogen molecules and carbon atoms [28]. To augment this, various heteroatoms such as nitrogen, boron, sulfur, and phosphorous can be introduced into the carbon structure via doping [29]. Here,

nitrogen doping is achieved through the mixing of melamine along with ZIF 67 before carbonization. This process alters the local electronic structure of the derived carbon matrix, potentially enhancing its hydrogen storage capabilities. The nitrogen doping in the carbon matrix causes a change in the local electronic structure of the carbon support in the Co/NC, Co/NC-0.3, Co/NC-0.5, and Co/NC-1 samples. The charge transfer between the modified electronic structure of the porous carbon matrix after the nitrogen doping and the embedded Co nanoparticles strengthens the interaction between these nanoparticles and the carbon support. This prevents the agglomeration of these Co nanoparticles over the porous carbon support and leads to uniform dispersion of nanoparticles due to the presence of nitrogen atoms. This could enhance the effective interaction of hydrogen molecules over these nanoparticles and thus improve the hydrogen storage capacity. The introduction of nitrogen atoms into carbon networks promotes charge transfer between adjacent carbon atoms, leading to improved hydrogen adsorption in porous ZIF 67-derived carbon matrix. This effect is further amplified by embedding Co metal nanoparticles, which enhances hydrogen uptake through the spillover mechanism [4, 30] Additionally, the structural defects created by nitrogen doping facilitate a more uniform distribution of Co nanoparticles within the porous carbon structure. The hydrogen storage capacity decreases in the following trend: Co/NC-0.5>Co/NC>Co/NC-1>Co/NC-0.3. The storage capacity for Co/NC-1 is reduced since there is a distortion of the sodalite cage structure of the ZIF -67 derived carbon, and there are much fewer Co nanoparticles embedded within such a support material. So, fewer hydrogen molecules will be involved in the spill-over mechanism, which leads to the degradation of the hydrogen adsorption performance. It is observed that Co/NC-0.3 also has less storage capacity compared to Co/NC, and this could be due to less coverage of nitrogen atoms within the porous sodalite cage structure of carbon matrix that is much necessary for anchoring of Co nanoparticles towards it. Co/NC-0.5 has the optimum amount of nitrogen distributed throughout the carbon surface, which is necessary for bonding Co nanoparticles on the carbon surface.



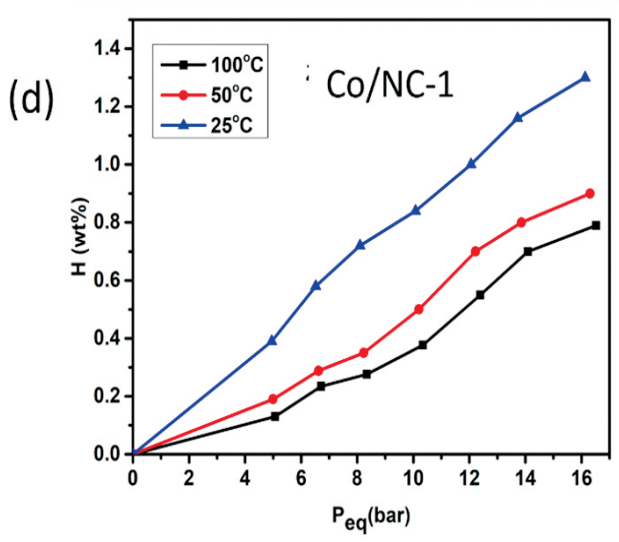


Fig. 9. PC isotherm plots of (a) Co/NC (b) Co/NC-0.3 (c) Co/NC-0.5 (d) Co/NC-1

A comparison with the other ZIF-derived carbon materials from the literature survey is shown in Table 2. A comparison of hydrogen storage performance with the other MOF-derived carbon materials

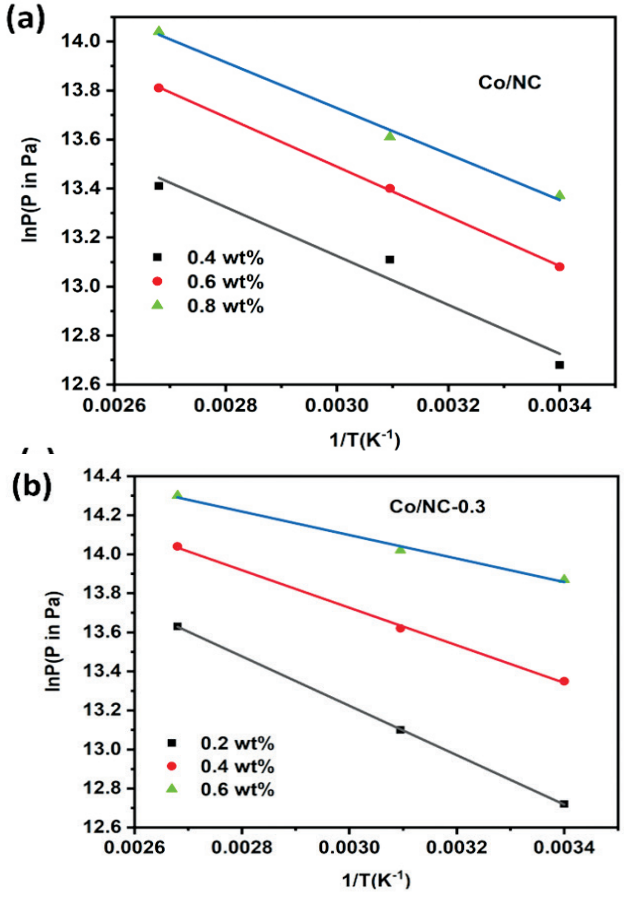
Samples	References	Pressure (bar)	Hydrogen uptake (wt%) (at 25°C)
ZIF67-derived carbon-500	[4]	~16	0.6
Pt/AC + Cu-TDPAT (MOF)	[31]	~1	0.044
MOF-derived carbon	[32]	~100	0.94
Pt@ZIF-8/GO	[33]	~10	0.841 (~77K)
MOF-5_b	[34]	~16	0.15 (~15 °C)
Co/NC-0.5 (ZIF 67 derived)	**This work**	~16	2.4

The isosteric heat of adsorption (Q_{st}) is obtained from the absolute heat of enthalpy, ΔH, which is acquired from the slope of the Van't Hoff plot. This plot is drawn between ln P (P in Pa) vs 1/T (K^{-1}) and its slope gives ΔH, at a fixed hydrogen storage capacity (in wt%) of the material. The Clausius-Clapeyron equation is used to quantify the strength of the contact between the hydrogen atoms and the sample's surface atoms [35] as follows:

Where R is the ideal gas constant, P is the H_2 equilibrium pressure, T is the temperature at which the amount of hydrogen stored (in wt %) is measured.

The isosteric heat of adsorption (Q_{st}) is calculated from the above equation after obtaining the slope from the Van't Hoff plots of Co/NC, Co/NC-0.3, Co/NC-0.5, and Co/NC-1, as shown in Fig 10 (a-d). Q_{st} values for Co/NC, Co/NC-0.3, Co/NC-0.5, and Co/NC-1, at different adsorption values 0.2 wt%, 0.4 wt%, 0.6 wt%, and 0.8 wt% are shown in Table 3 below.

Any carbon-based adsorbent is said to have an enthalpy of adsorption of 4-6 $kJmol^{-1}$, which is extremely low to meet the requirements for hydrogen storage material at room temperature [36]. Enthalpy of adsorption equivalent to or less than 15 $kJmol^{-1}$ is desired in materials to achieve the DOE requirement for an effective hydrogen storage material [37]. This is closely achieved by Co/NC-0.5, which shows an isosteric heat of adsorption value of 11.21 $kJmol^{-1}$, as seen in Table 3.



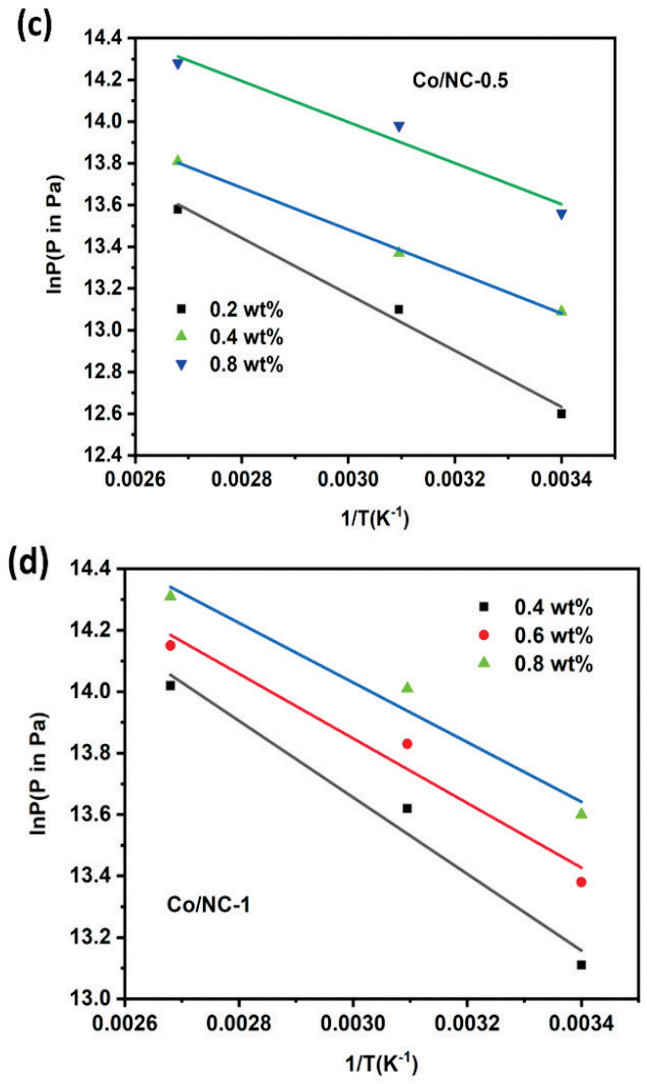


Fig 10 Van't Hoff plots of (a) Co/NC (b) Co/NC-0.3 (c) Co/NC-0.5 (d) Co/NC-1

Table -3. Comparison of Q_{st} values of Co/NC, Co/NC-0.3, Co/NC-0.5 and Co/NC-1

Sample	Q_{st} at 0.2 wt% ($kJmol^{-1}$)	Q_{st} at 0.4 wt% ($kJmol^{-1}$)	Q_{st} at 0.6 wt% ($kJmol^{-1}$)	Q_{st} at 0.8 wt% ($kJmol^{-1}$)
Co/NC	-	8.2	8.4	7.7
Co/NC-0.3	10	7.9	5	-
Co/NC-0.5	11.2	8.5	-	8.1
Co/NC-1	-	9	8.5	8

4. Conclusions

ZIF 67 was used as the source of Co/NC, Co/NC-0.3, Co/NC-0.5, and Co/NC-1, which were synthesized utilizing a straightforward, cost-effective pyrolysis synthesis method employing varying amounts of melamine. XRD was used to confirm the phases of the embedded Co nanoparticles within the nitrogen-doped porous carbon, while SEM and EDAX measurements were used to establish the structure and elemental composition. BET measurement is performed to determine each sample's specific surface area (SSA) and pore size distribution. Compared to Co/NC, Co/NC-0.3, and Co/NC-1, the hydrogen adsorption capacity of Co/NC-0.5 is higher. This is because of the complementary effects of the right concentration of nitrogen and metal embedment, which increase the number of active sites available for the H atom's adsorption through the spillover process. For effective hydrogen adsorption, the addition of 0.5 mmol of melamine results in a homogeneous dispersion of metal nanoparticles in the carbon matrix and strengthens the metal-nitrogen-carbon link. Every sample's ability to store hydrogen follows this general pattern: Co/NC-0.5>Co/NC>Co/NC-1>Co/NC-0.3 in the 25–100°C temperature range and 5–16 bar pressure range. This paper reports the maximum hydrogen storage capacity for Co/NC-0.5 at room temperature and at an H_2 equilibrium pressure of around 16 bar, which is 2.45 wt%. Additionally, Co/NC-0.5 exhibits the greatest Qst value (11.2 $kJmol^{-1}$), which is quite near to the targeted DOE value of 15 $kJmol^{-1}$. Out of all the several kinds of ZIF-derived carbon, this has the largest hydrogen storage capacity at room temperature. The significant increase in modified porous carbon's storage capacity, while still far short of the US DOE target of 6wt% hydrogen storage capacity, opens the door for the development of hydrogen storage adsorption systems, ideally at ambient conditions.

Acknowledgments

The authors wish to thank MHRD, Govt. of India, Department of Science and Technology (DST) for the financial support.

References

[1] L. Schlapbach et A. Züttel, Hydrogen-storage materials for mobile applications, vol. 414, 2001, [En ligne]. Disponible à: www.nature.com

[2] S. J. Yang *et al.*, MOF-derived hierarchically porous carbon with exceptional porosity and hydrogen storage capacity, *Chemistry of Materials*, vol. 24, nº 3, p. 464-470, févr. 2012, doi: 10.1021/cm202554j.

[3] H. Furukawa, K. E. Cordova, M. O'Keeffe, et O. M. Yaghi, « The chemistry and applications of metal-organic frameworks, *Science*, vol. 341, nº 6149. American Association for the Advancement of Science, 2013. doi: 10.1126/science.1230444.

[4] P. Sen Tseng *et al.*, ZIF-67 derived Co nanoparticles on ZIF-Derived carbon for hydrogen spillover and storage, *Appl Surf Sci*, vol. 638, nov. 2023, doi: 10.1016/j.apsusc.2023.158097.

[5] H. Reardon, J. M. Hanlon, R. W. Hughes, A. Godula-Jopek, T. K. Mandal, et D. H. Gregory, Emerging concepts in solid-state hydrogen storage: The role of nanomaterials design, *Energy and Environmental Science*, vol. 5, nº 3. p. 5951-5979, mars 2012. doi: 10.1039/c2ee03138h.

[6] Q. Wang *et al.*, Highly active cobalt- and nitrogen-doped carbon derived from ZIF-67@melamine towards oxygen reduction reaction, *Journal of Electroanalytical Chemistry*, vol. 894, août 2021, doi: 10.1016/j.jelechem.2021.115397.

[7] B. Liu, H. Shioyama, T. Akita, et Q. Xu, Metal-organic framework as a template for porous carbon synthesis, *J Am Chem Soc*, vol. 130, nº 16, p. 5390-5391, avr. 2008, doi: 10.1021/ja7106146.

[8] M. Kim *et al.*, MOF-derived nanoporous carbons with diverse tunable nanoarchitectures, *Nat Protoc*, vol. 17, nº 12, p. 2990-3027, déc. 2022, doi: 10.1038/s41596-022-00718-2.

[9] A. Nuhnen et C. Janiak, A practical guide to calculate the isosteric heat/enthalpy of adsorption: Via adsorption isotherms in metal-organic frameworks, MOFs, *Dalton Transactions*, vol. 49, nº 30. Royal Society of Chemistry, p. 10295-10307, 14 août 2020. doi: 10.1039/d0dt01784a.

[10] V. F. Yusuf, N. I. Malek, et S. K. Kailasa, Review on Metal-Organic Framework Classification, Synthetic Approaches, and Influencing Factors: Applications in Energy, Drug Delivery, and Wastewater Treatment, *ACS Omega*, vol. 7, nº 49. American Chemical Society, p. 44507-44531, 13 décembre 2022. doi: 10.1021/acsomega.2c05310.

[11] F. Zheng *et al.*, Review: Synthesis and Catalytic Application of MOF Complexes Containing Noble Metals, *Energy and Fuels*. American Chemical Society, 2024. doi: 10.1021/acs.energyfuels.4c01963.

[12] H. Konnerth, B. M. Matsagar, S. S. Chen, M. H. G. Prechtl, F. K. Shieh, et K. C. W. Wu, Metal-organic framework (MOF)-derived catalysts for fine chemical production, *Coordination Chemistry Reviews*, vol. 416. Elsevier B.V., 1 août 2020. doi: 10.1016/j.ccr.2020.213319.

[13] S. Lu *et al.*, Hydrogenation of furfural over Pd@ZIF-67 derived catalysts: direct hydrogenation and transfer hydrogenation, *New Journal of Chemistry*, vol. 46, nº 28, p. 13715-13724, juin 2022, doi: 10.1039/d2nj01565j.

[14] K. Murugesan *et al.*, Cobalt-based nanoparticles prepared from MOF-carbon templates as efficient hydrogenation catalysts, *Chem Sci*, vol. 9, nº 45, p. 8553-8560, 2018, doi: 10.1039/c8sc02807a.

[15] S. Yang *et al.*, MOF-Derived Cobalt Phosphide/Carbon Nanocubes for Selective Hydrogenation of Nitroarenes to Anilines, *Chemistry - A European Journal*, vol. 24, nº 17, p. 4234-4238, mars 2018, doi: 10.1002/chem.201705400.

[16] Q. Su, Q. Guo, H. Wang, M. Liu, et C. Zuo, Research progress of MOF-based materials in the photocatalytic CO2 reduction, *Carbon Resources Conversion*, vol. 7, nº 1. KeAi Publishing Communications Ltd., 1 mars 2024. doi: 10.1016/j.crcon.2023.100211.

[17] A. Li, R. F. Lu, Y. Wang, X. Wang, K. L. Han, et W. Q. Deng, Lithium-doped conjugated microporous polymers for reversible hydrogen storage, *Angewandte Chemie - International Edition*, vol. 49, nº 19, p. 3330-3333, avr. 2010, doi: 10.1002/anie.200906936.

[18] C. S. Tsao *et al.*, « Hydrogen spillover effect of pt-doped activated carbon studied by inelastic neutron scattering », *Journal of Physical Chemistry Letters*, vol. 2, nº 18, p. 2322-2325, sept. 2011, doi: 10.1021/jz2010368.

[19] S. Fathima T.K., A. Ghosh, et S. Ramaprabhu, ZIF67-derived Co–CoO@C nanocomposites as highly efficient and selective oxygen evolution reaction (OER) catalysts for seawater electrolysis, *Int J Hydrogen Energy*, vol. 49, p. 780-793, janv. 2024, doi: 10.1016/j.ijhydene.2023.09.122.

[20] J. Qian, F. Sun, et L. Qin, Hydrothermal synthesis of zeolitic imidazolate framework-67 (ZIF-67) nanocrystals, *Mater Lett*, vol. 82, p. 220-223, sept. 2012, doi: 10.1016/j.matlet.2012.05.077.

[21] B. Weng *et al.*, Metal-Organic Framework-Derived CoWP@C Composite Nanowire Electrocatalyst for Efficient Water Splitting, *ACS Energy Lett*, vol. 3, nº 6, p. 1434-1442, juin 2018, doi: 10.1021/acsenergylett.8b00584.

[22] M. Afkhami-Ardekani, M. R. Naimi-Jamal, S. Doaee, et S. Rostamnia, Solvent-Free Mechanochemical Preparation of Metal-Organic Framework ZIF-67 Impregnated by Pt Nanoparticles for Water Purification, *Catalysts*, vol. 13, nº 1, janv. 2023, doi: 10.3390/catal13010009.

[23] Y. Xu *et al.*, (Co, Ni)-NC/CNT Composite as a Cathode for Li-S Batteries, *ACS Appl Nano Mater*, vol. 7, nº 9, p. 10520-10531, mai 2024, doi: 10.1021/acsanm.4c00955.

[24] A. R. Dhanya, P. Haridoss, et R. Sundara, EDA/PANI derived FeNxC with Fe-Nx active sites as room temperature hydrogen storage material, *J Alloys Compd*, vol. 970, janv. 2024, doi: 10.1016/j.jallcom.2023.172596.

[25] R. Das, P. Pachfule, R. Banerjee, et P. Poddar, Metal and metal oxide nanoparticle synthesis from metal organic frameworks (MOFs): Finding the border of metal and metal oxides, *Nanoscale*, vol. 4, nº 2, p. 591-599, janv. 2012, doi: 10.1039/c1nr10944h.

[26] A. R. Dhanya, N. Ranjan, et S. Ramaprabhu, Hydrogen storage studies of Co, Fe, Fe3C nanoparticles encapsulated nitrogen doped carbon nanotubes, *Energy Storage*, vol. 5, nº 4, juin 2023, doi: 10.1002/est2.421.

[27] S. S. Samantaray, V. Sangeetha, S. Abinaya, et S. Ramaprabhu, Diatom frustule-graphene based nanomaterial for room temperature hydrogen storage, *Int J Hydrogen Energy*, vol. 45, nº 1, p. 764-773, janv. 2020, doi: 10.1016/j.ijhydene.2019.10.155.

[28] A. Gupta *et al.*, Hydrogen Clathrates: Next Generation Hydrogen Storage Materials, *Energy Storage Materials*, vol. 41. Elsevier B.V., p. 69-107, 1 octobre 2021. doi: 10.1016/j.ensm.2021.05.044.

[29] Y. Xia, G. S. Walker, D. M. Grant, et R. Mokaya, Hydrogen storage in high surface area carbons: Experimental demonstration of the effects of nitrogen doping, *J Am Chem Soc*, vol. 131, nº 45, p. 16493-16499, 2009, doi: 10.1021/ja9054838.

[30] A. P. Pandey, M. A. Shaz, V. Sekkar, et R. S. Tiwari, Synergistic effect of CNT bridge formation and spillover mechanism on enhanced hydrogen storage by iron doped carbon aerogel, *Int J Hydrogen Energy*, vol. 48, nº 56, p. 21395-21403, juill. 2023, doi: 10.1016/j.ijhydene.2022.02.076.

[31] C. Y. Wang *et al.*, Hydrogen storage with spectroscopic identification of chemisorption sites in Cu-TDPAT via spillover from a Pt/activated carbon catalyst, *Journal of Physical Chemistry C*, vol. 118, nº 46, p. 26750-26763, nov. 2014, doi: 10.1021/jp507395p.

[32] S. J. Yang *et al.*, MOF-derived hierarchically porous carbon with exceptional porosity and hydrogen storage capacity, *Chemistry of Materials*, vol. 24, nº 3, p. 464-470, févr. 2012, doi: 10.1021/cm202554j.

[33] H. Zhou, J. Zhang, D. Ji, A. Yuan, et X. Shen, Effect of catalyst loading on hydrogen storage capacity of ZIF-8/graphene oxide doped with Pt or Pd via spillover, *Microporous and Mesoporous Materials*, vol. 229, p. 68-75, juill. 2016, doi: 10.1016/j.micromeso.2016.04.007.

[34] S. M. Luzan et A. V. Talyzin, Hydrogen adsorption in Pt catalyst/MOF-5 materials, *Microporous and Mesoporous Materials*, vol. 135, nº 1-3, p. 201-205, 2010, doi: 10.1016/j.micromeso.2010.07.018.

[35] Q. R. Zheng, S. Gao, et C. J, Determination of the isosteric heat of adsorption of hydrogen on the Multi-Walled Carbon Nanotubes, dans *Advanced Materials Research*, 2012, p. 1484-1491. doi: 10.4028/www.scientific.net/AMR.512-515.1484.

[36] E. W. Knight *et al.*, Determination of the Enthalpy of Adsorption of Hydrogen in Activated Carbon at Room Temperature, 2020. [En ligne]. Disponible à: https://www.elsevier.com/open-access/userlicense/1.0/

[37] S. S. Samantaray, V. Sangeetha, S. Abinaya, et S. Ramaprabhu, Enhanced hydrogen storage performance in Pd3Co decorated nitrogen/boron doped graphene composites, *Int J Hydrogen Energy*, vol. 43, nº 16, p. 8018-8025, avr. 2018, doi: 10.1016/j.ijhydene.2018.03.078.